Steel and Composite Structures, *Vol. 21, No. 5 (2016) 1045-1067*
DOI: http://dx.doi.org/10.12989/scs.2016.21.5.1045

Prestressed concrete bridges with corrugated steel webs: Nonlinear analysis and experimental investigation

Xia-chun Chen [1], Zhi-zhou Bai [1,2], Yu Zeng [1], Rui-juan Jiang [1,3] and Francis T.K. Au [*1]

[1] *Department of Civil Engineering, The University of Hong Kong, Hong Kong, China*
[2] *Department of Bridge Engineering, Tongji University, Shanghai, 200092, China*
[3] *Research Center, Shenzhen Municipal Engineering Design and Research Institute, Shenzhen, 518029, China*

(*Received October 26, 2015, Revised June 20, 2016, Accepted July 22, 2016*)

Abstract. Concrete bridges with corrugated steel webs and prestressed by both internal and external tendons have emerged as one of the promising bridge forms. In view of the different behaviour of components and the large shear deformation of webs with negligible flexural stiffness, the assumption that plane sections remain plane may no longer be valid, and therefore the classical Euler-Bernoulli and Timoshenko beam models may not be applicable. In the design of this type of bridges, both the ultimate load and ductility should be examined, which requires the estimation of full-range behaviour. An analytical sandwich beam model and its corresponding beam finite element model for geometric and material nonlinear analysis are developed for this type of bridges considering the diaphragm effects. Different rotations are assigned to the flanges and corrugated steel webs to describe the displacements. The model accounts for the interaction between the axial and flexural deformations of the beam, and uses the actual stress-strain curves of materials considering their stress path-dependence. With a nonlinear kinematical theory, complete description of the nonlinear interaction between the external tendons and the beam is obtained. The numerical model proposed is verified by experiments.

Keywords: corrugated steel webs; full-range behaviour; geometric nonlinearity; material nonlinearity; prestressed concrete bridges; sandwich beam theory

1. Introduction

The prestressed concrete bridge with corrugated steel webs is a structural form in which the steel webs mainly resist shear force and the concrete flanges mainly resist bending moment. Corrugated steel webs provide high shear buckling resistance and high transverse stiffness without the need for stiffeners as in conventional flat steel webs. The omission of stiffeners facilitates easy maintenance. Extensive analyses of the local, global and interactive buckling of corrugated steel webs show that they have reasonable post-buckling shear capacities and are also less prone to geometric imperfection. Owing to the high buckling strength, corrugated steel webs can be thinner than conventional flat steel webs. Because of the so-called "accordion effect", the axial stiffness of corrugated steel webs is negligible and hence prestress can be introduced efficiently to the concrete flanges. The thin steel webs enable substantial weight reduction and hence longer spans

*Corresponding author, Professor, E-mail: francis.au@hku.hk

Copyright © 2016 Techno-Press, Ltd.
http://www.techno-press.org/?journal=scs&subpage=6 ISSN: 1229-9367 (Print), 1598-6233 (Online)

than those of bridges with conventional concrete webs. To further reduce the weight, high strength concrete can be used for the flanges. The light weight of this bridge form makes it ideal not only for girder bridges on their own but also as the deck in cable-stayed bridges. This structural form provides both excellent structural efficiency and elegant appearance. In 1986, the first bridge of this type, Cognac Bridge, was built in France (Cheyrezy and Combault 1990). The successful application and its significant advantages over the conventional prestressed concrete bridge has prompted researchers and construction companies in various countries, including Japan, USA, China and Germany, to get involved in this new composite structure. Hereafter in this paper, this form of bridge is assumed unless otherwise stated.

Despite various merits brought by the corrugated steel webs, there are also some concerns in this type of bridges. These bridges are known to have lower stiffness than those with conventional concrete or flat steel webs, which leads to larger deflections. Even though some initial design guidance has been formulated (Research Group of Composite Structure with Corrugated Steel Web 1998), there are still various issues to resolve. In view of the rotational difference between the deformed flange sections and web section, the assumption that plane sections remain plane is not valid, and the classical Euler-Bernoulli and Timoshenko beam theories do not apply (Machimdamrong *et al*. 2004). To model the behaviour, Taniguchi and Yoda (1997) proposed a simple numerical method based on a laminated beam theory. Kato *et al*. (2002) later carried out analysis assuming the corrugated steel webs to carry shear force only and the flanges to resist all the bending moment involving the independent displacement fields of deflection and rotation of the web section, but the shear force in flanges was underestimated. Using the variational principle, Machimdamrong *et al*. (2004) developed a more precise extended elastic shear deformable beam theory, or G3 theory, involving three independent displacement fields covering deflection, rotation of flange sections, and relative displacement of the upper and lower flanges. Xu *et al*. (2015) studied the structural behaviour using spatial grid modelling. For this type of bridges, due to the negligible axial stiffness but remarkable shear deformation of corrugated steel webs, the diaphragms have significant effects on the bending behaviour of the bridge by constraining the web shear deformation in its vicinity and preventing relative longitudinal movement of the flanges. Chen *et al*. (2015b) outlined an extended sandwich beam model taking into account the diaphragm effects to predict elastic behaviour of the bridges. The above models mainly focus the elastic behaviour.

However, relatively little work has been done on the full-range behaviour. In the design of this type of bridges, both the ultimate load and ductility should be carefully examined, which requires the estimation of full-range behaviour. Bariant and Utsunomiya (2006) extended the G3 theory to the elasto-plastic stage accounting for the inelastic properties of steel webs. To fully understand the full-range behaviour, the material nonlinearities of concrete, steel webs, non-prestressed and prestressing steel, the geometric nonlinearities, and the second-order effects associated with external tendons also need to be considered. The buckling strength of corrugated steel webs has been widely studied, e.g., Barakat *et al*. (2015). Experimental investigations of this type of bridges have been carried out by Mizuguchi *et al*. (1998), Mo *et al*. (2003), Kosa *et al*. (2006), etc. Mo *et al*. (2003) predicted the full-range load-displacement relationship of such box-girders by the moment area method and the curvature diagram. Ko *et al*. (2013) carried out nonlinear analysis on the torsion behaviour by a three-dimensional finite element model. The full-range behaviour of these bridges is rather complicated due to material and geometric nonlinearities, interaction among components of different properties, presence of external prestressing tendons and diaphragms, etc. A simple but reliable model for nonlinear structural analysis, considering the effects of external

tendons and diaphragms, is needed for this type of bridges.

The plastic zone model proposed by Park and Paulay (1975) is widely adopted in nonlinear structural analysis of conventional concrete beams, e.g. Ho and Pam (2003), Au *et al*. (2005), Du *et al*. (2008), Eslami and Ronagh (2014), and Youssf *et al*. (2015). However, in the plastic zone model the equivalent plastic hinge length needs to be assumed in advance. For this type of bridges, owing to violation of the assumption that plane sections remain plane, the equivalent length of plastic hinge is still uncertain. Detailed finite element models are also widely adopted for conventional concrete bridges, e.g. Lou and Xiang (2006), Dall'Asta *et al*. (2007), Zona *et al*. (2008), and Zona and Ranzi (2011). In the detailed finite element model, the bridge beam is divided into a number of elements along the axis. The elements are based on the fibre stress-strain relationships determined by equilibrium and compatibility requirements.

In this study, the sandwich model proposed by Chen *et al*. (2015b) is adopted and extended to nonlinear stage predict the full-range behaviour of the bridges taking into account geometric and material nonlinearities, and the interactions between beam, diaphragm and external prestressing tendons.

2. Theoretical formulation

The following assumptions are made for the theoretical formulation: (a) The shear deformation of the concrete flanges is negligible; (b) The flexural rigidity of the webs is negligible (Johnson and Cafolla 1997); (c) The beam is incompressible vertically; (d) The shear lag effect is disregarded in the present study; (e) The stress-strain curves of concrete, non-prestressed and prestressing steel are as given by the constitutive models; (f) Deflections may be large but rotations are small to moderate; (g) The relative interface slip between external tendons and deviators are allowed; (h) The corrugated steel webs are perfectly bonded with the concrete flanges; and (i) The flexural failure occurs before shear buckling of corrugated steel webs and shear connection failure.

2.1 Beam model

The behaviour of this type of bridge is similar to that of a sandwich beam with thick facings as shown in Fig. 1. Both the core of the sandwich beam and the corrugated steel webs have negligible flexural rigidities. The present theory is developed as a two-dimensional theory with the beam axis denoted as x-axis and the vertical direction along beam depth denoted as z-axis, as shown in Fig. 2. Referring to the typical cross section of bridge as shown in Fig. 2(a), t_u and t_l are the depths of upper and lower flanges respectively; b_u and b_l are the widths of upper and lower flanges respectively; h_w is the height of web; h is the distance between centroidal axes of flanges; and e_u and e_l are the distances from the centroidal axis of entire beam section to the centroidal axes of upper and lower flanges respectively. Fig. 2(b) shows typical forms of corrugated web (trapezoidal and sinusoidal) where s denotes the developed length of a half corrugation; s_0 denotes its projected length; r denotes the rise of corrugation; and θ denotes the trough angle.

The analysis of corrugated steel sheets is often carried out by using the theory of orthotropic plates, which has been verified to be adequate for the essential structural behaviour. According to Briassoulis (1986) and Samanta and Mukhopadhyay (1999), the equivalent orthotropic shear modulus G_e of the corrugated web is given by

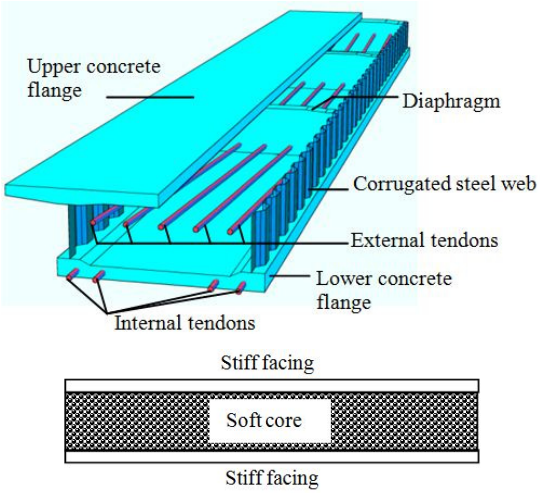

Fig. 1 Comparison of (a) a bridge; and (b) a sandwich beam with thick faces

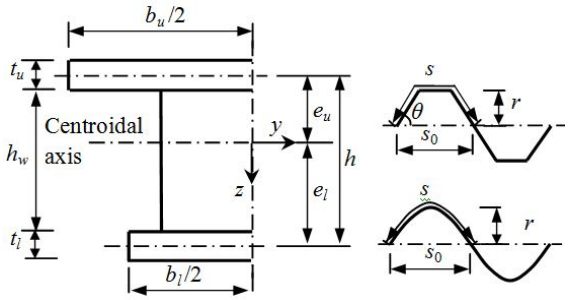

Fig. 2 A cross section of bridge and typical web corrugations: (a) a typical section; and (b) typical web corrugations

$$G_e = \frac{s_0}{s} G_w \tag{1}$$

where G_w is the shear modulus of material of the corrugated web.

For this type of bridges, the bending deflection v_1 and shear deflection v_2 cannot be superimposed without considering their interaction, as illustrated by the simply-supported bridge under a point load at mid-span. Ignoring the local bending stiffnesses of flanges initially, shear deflection v_2 would occur as shown in Fig. 3, which would induce excessive local bending stresses in the flanges at the kink. As it is impossible for the flanges to bend to an infinite curvature at mid-span, the flanges bend locally and smooth out the kink of shear deflection. Actually interaction does occur thereby resulting in additional local curvature v_2'' of the flanges, giving rise to additional shear force and bending moment. This is considered as the interaction between shear deformation of corrugated steel webs and local bending of concrete flanges.

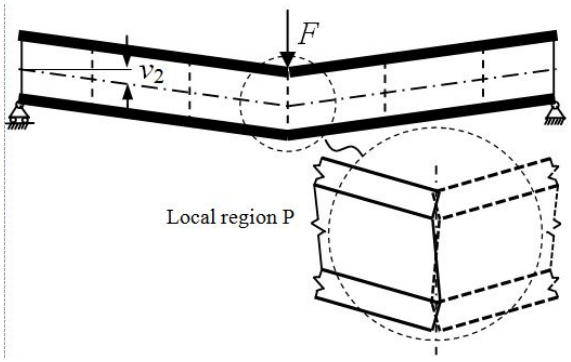

Fig. 3 Shear deflection ignoring local bending of flanges of a bridge under a point load at mid-span

Referring to the beam segment as shown in Fig. 4, the flange displacement u_f in the x-direction is given by

$$u_f = u + e_f\varphi - \left(z - e_f\right)\frac{\partial v}{\partial x} \tag{2}$$

where u is the longitudinal displacement of the axis of the beam; e_f is the z-value of the axis of the flange considered; φ is the normal rotation of the section based on the centroids of flanges; and v is the total deflection of the beam. By introducing geometric nonlinearity, the strain of a generic fiber of the flange in the deformed configuration can be obtained by

$$\varepsilon_f = \frac{\partial u_f}{\partial x} + \frac{1}{2}\left(\frac{\partial v}{\partial x}\right)^2 = \varepsilon_0 + \left[e_f\frac{\partial \varphi}{\partial x} - \left(z - e_f\right)\frac{\partial^2 v}{\partial x^2}\right] \tag{3}$$

where $\varepsilon_0 = u' + (1/2)(v')^2$ is the strain of the beam axis and the term $(1/2)(v')^2$ is due to geometric nonlinearity. The above equation is based on assumptions of large transverse deflection and small to moderate rotations, which are widely adopted (Reddy 2004) and acceptable for bridge structures (Dall'Asta *et al*. 2007).

The shear strain, γ_w, of the webs is given by

$$\gamma_w = \frac{\partial v}{\partial x} + \frac{\partial u_w}{\partial z} \tag{4}$$

where u_w is the displacement of any point in the steel webs in the x-direction. By considering the displacement patterns of φ and $\partial v/\partial x$ as shown in Fig. 4, one can obtain

$$\frac{\partial u_w}{\partial z} = \frac{u_f\big|_{z=e_l - t_l/2} - u_f\big|_{z=-e_u + t_u/2}}{h_w} = \frac{h\varphi + \left(\frac{t_l}{2} + \frac{t_u}{2}\right)\frac{\partial v}{\partial x}}{h_w} \tag{5}$$

Substituting Eq. (5) into Eq. (4) and further rearrangement yield

$$\gamma_w = \beta\gamma = \beta\left(\varphi + \partial v/\partial x\right) \tag{6}$$

where $\beta = h/h_w$; and γ is the equivalent shear strain of the entire section that is given by

$$\gamma = \varphi + \partial v/\partial x \tag{7}$$

The virtual strain energy δU_b in the flanges and webs of the beam is given by

$$\begin{aligned}
\delta U_b &= \int_L\int_{A_f}\sigma_f\delta\varepsilon_f \mathrm{d}A_f\mathrm{d}x + \int_L\int_{A_w}\tau_w\delta\gamma_w\mathrm{d}A_w\mathrm{d}x \\
&= \int_L\int_{A_f}\sigma_f\left\{\delta\varepsilon_0 + e_f\frac{\partial\delta\varphi}{\partial x} + \left(z - e_f\right)\left(-\frac{\partial^2\delta v}{\partial x^2}\right)\right\}\mathrm{d}A_f\mathrm{d}x + \int_L\int_{A_w}\tau_w\delta\gamma_w\mathrm{d}A_w\mathrm{d}x \\
&= \int_L N\delta\varepsilon_0\mathrm{d}x + \int_L M_g\frac{\partial\delta\varphi}{\partial x}\mathrm{d}x + \int_L M_{loc}\left(-\frac{\partial^2\delta v}{\partial x^2}\right)\mathrm{d}x + \int_L V_w\delta\gamma_w\mathrm{d}x
\end{aligned} \tag{8}$$

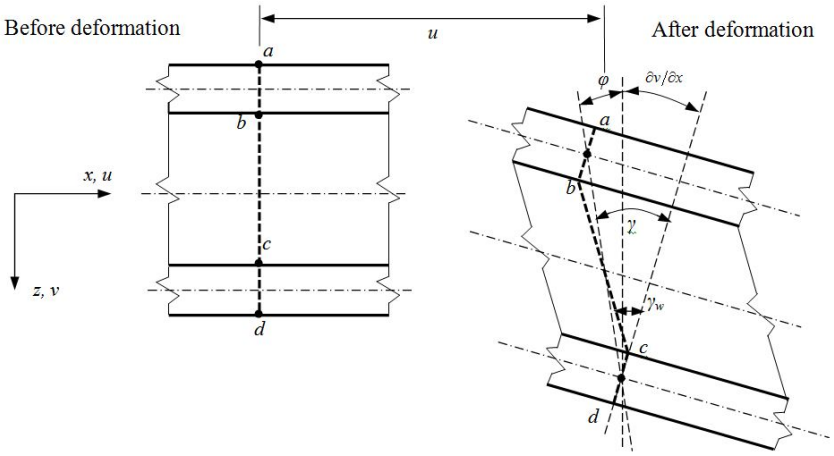

Fig. 4 Deformation of a beam segment

where A_f and A_w are areas the flanges and webs respectively; σ_f and τ_w are the normal stress and shear stress of the flanges and webs respectively; and the axial force N, the global bending moment M_g about the centroidal axis of the entire beam assuming uniform stress in each flange, the sum of local bending moments of flanges about their respective axes M_{loc}, and the shear force V_w carried by the corrugated steel webs are given respectively by

$$N = \int_{A_f} \sigma_f \mathrm{d}A_f , \tag{9a}$$

$$M_g = \int_{A_f} \sigma_f e_f \mathrm{d}A_f , \tag{9b}$$

$$M_{loc} = \int_{A_f} \sigma_f \left(z - e_f\right) \mathrm{d}A_f , \tag{9c}$$

$$V_w = \int_{A_w} \tau_w \mathrm{d}A_w \tag{9d}$$

The total shear force V acting on the section perpendicular to the deformed beam can be given by the sum of local shear force V_{loc} associated with the local bending stiffnesses of the flanges about their respective axes and the global shear force V_g associated with global bending stiffness of the flanges about the axis of the entire beam section assuming uniform stress in each flange, i.e.

$$V = V_g + V_{loc} \tag{10}$$

Obviously, the sum of local shear force V_{loc} can be given in terms of the associated sum of local bending moments M_{loc} by

$$V_{loc} = \partial M_{loc} / \partial x \tag{11}$$

As the flexural rigidity of the webs is negligible, the shear stress of the webs τ_w is uniform across the height giving a uniform shear flow. As opposed to common sandwich beams, this type of bridge consists of narrow webs and relatively wide flanges, therefore resulting in complicated

distribution of shear stresses especially at the web-flange junctions. For simplicity, the present derivation is based on the assumption of thin-walled section, which should be reasonably accurate (Timoshenko and Gere 1972). Hence assuming the same shear flow to apply from the lower web-flange junction to the top web-flange junction, the global shear force can be estimated as

$$V_g = \beta V_w \tag{12}$$

The total shear force V_z on a section perpendicular to the x-axis is therefore given by

$$V_z = V + N\left(\partial v/\partial x\right) \tag{13}$$

2.2 Effects of diaphragms

These bridges are often provided with end and intermediate diaphragms. As the axial stiffness of corrugated steel web is negligible but its shear deformation is remarkable, the diaphragms have significant effects on the bending behaviour of the bridge by constraining the web shear deformation in its vicinity and preventing relative longitudinal movement of the flanges as shown in Fig. 5, thereby further integrating various components together for higher efficiency.

The effects of diaphragms can be considered by imposing additional boundary or compatibility conditions. For convenience, the diaphragms are assumed to be thin-walled members located at their centrelines and monolithic with the webs and flanges. For the compatibility condition, the relative longitudinal movement of the diaphragm Δ_d can be given by

$$\Delta_d = h_w \beta\left(\varphi + \partial v/\partial x\right) \tag{14}$$

The equilibrium condition is written as

$$K_d \Delta_d h = M_g^{(+)} - M_g^{(-)} \tag{15}$$

where K_d is the equivalent stiffness of the diaphragm associated with Δ_d; and the superscripts $^{(-)}$ and $^{(+)}$ denote quantities at the left and right of the diaphragm respectively. Combining the compatibility condition Eq. (14) and equilibrium condition Eq. (15), the additional condition at each diaphragm is obtained as

$$K_d h_w \beta\left(\varphi + \partial v / \partial x\right) h = M_g^{(+)} - M_g^{(-)} \tag{16}$$

The action of the diaphragm can be considered as a force couple of $K_d h_w \beta\ (\varphi + \partial v / \partial x) h$ from Eq. (16). The virtual strain energy associated with the diaphragms δU_{dia} is given by

$$\delta U_{dia} = \sum_k \left\{ \left[K_d h_w \beta \left(\varphi + \frac{\partial v}{\partial x} \right) h \right] \left(\delta\varphi + \frac{\partial \delta v}{\partial x} \right) \right\}_{x = x_k} \tag{17}$$

where x_k is the x-value to define the location of the kth diaphragm and the symbol δ denotes virtual quantities.

If the diaphragm is thick, it may be more appropriate to consider the diaphragm as a beam segment with solid section along the span.

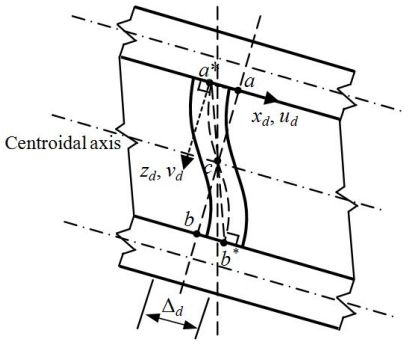

Fig. 5 Shear deformation of the bridge in the vicinity of a diaphragm

In essence, the diaphragm effect can be taken as a type of local interaction between shear deformation and local bending of flanges.

2.3 Modelling of external tendons

In the elastic stage, the increase of tendon force due to the small deformation of the structural system is negligible. For simplification in this case, only the initial prestressing force can be considered by applying the equivalent nodal forces for analysis. However, when the structure enters the cracked elastic and plastic stages, the increase in tendon force becomes significant. The external tendons interact with the beam through anchorages and deviators, as the tendon elongation depends on the global deformation of the whole structural system. The relative slip between external tendons and deviators can be considered free in most practical cases. Dall'Asta *et al*. (2007) developed a model for the external tendons of prestressed Euler-Bernoulli beams with a nonlinear kinematical theory and provided a complete description of the nonlinear interaction between external tendons and beam. This model is further extended and modified for this type of bridges.

The profile of external prestressing tendon is defined by the locations of end anchorages and intermediate deviators. Each location point, $\mathbf{c}_{0,j}$, can be expressed as

$$\mathbf{c}_{0,j} = x_j \mathbf{i} + e_j \mathbf{k} \tag{18}$$

where **i** and **k** are unit vectors parallel to x- and z-axis respectively; and x_j and e_j are the x-value and eccentricity, respectively, of the j-th location point with a deviator or anchorage (j=0, 1, 2…n). The initial total length of the tendon L_{t0} can be given by

$$L_{t0} = \sum_{j=1}^{n} \left| \mathbf{c}_{0,j} - \mathbf{c}_{0,j-1} \right| \tag{19}$$

After deformation, the location point $\mathbf{c}_{0,j}$ moves to a new position $\mathbf{c}_j$ of

$$\mathbf{c}_j = \left[x_j + u_j + e_j \varphi_j \right] \mathbf{i} + \left[e_j + v_j \right] \mathbf{k} \tag{20}$$

where u_j, v_j and φ_j are the displacements at x_j. The total length of the tendon after deformation L_t is given by

$$L_t = \sum_{j=1}^{n} \left| \mathbf{c}_j - \mathbf{c}_{j-1} \right| \tag{21}$$

The additional elongation ΔL_t of the external tendon is then obtained as $\Delta L_i = Li - L_{i0}$.

Assuming that the strain ε_p of the external tendon remains small if the inclination of the tendon profile is moderate, the tendon deformation measured in its deformed configuration can be simplified as

$$\varepsilon_p = \frac{\Delta L_t}{L_{t0}} \approx \frac{1}{L_{t0}} \sum_{j=1}^{n} \left\{ \frac{1}{2} \frac{\left(\Delta_j e + \Delta_j v \right)^2}{l_{p,j}} + \frac{\Delta_j x}{l_{p,j}} \left[\Delta_j x + \Delta_j u + \Delta_j \left(e\varphi \right) \right] \right\} - 1 \tag{22}$$

where $\Delta_j(\bullet) = (\bullet)_j - (\bullet)_{j-1}$; and $l_{p,j} = \sqrt{(\Delta_j x)^2 + (\Delta_j e)^2}$. The assumption made here is acceptable if the tendon profile is within the beam depth as in most cases (Dall'Asta *et al*. 2007). Consequently, the virtual strain of the external tendon is given by

$$\delta\varepsilon_p = \frac{1}{L_{t0}} \sum_{j=1}^{n} \left\{ \frac{\left(\Delta_j e + \Delta_j v \right)}{l_{p,j}} \Delta_j \delta v + \frac{\Delta_j x}{l_{p,j}} \left[\Delta_j \delta u + \Delta_j \left(e\delta\varphi \right) \right] \right\} \tag{23}$$

The virtual strain energy δU_p associated with the external tendon can be obtained by

$$\delta U_p = L_{t0} A_p \sigma_p \delta\varepsilon_p \tag{24}$$

For simplification for illustration, only one resultant external tendon is considered hereafter. Straightforward generalization to cases with more external tendons can be achieved by superposition.

2.4 Global structural system

There are interactions between the beam, diaphragms and external tendons in the structural system. The global behaviour of the whole structural system can be obtained by the principle of virtual work as

$$\delta U_b + \delta U_p + \delta U_{dia} = \delta W_E \tag{25}$$

where δW_E is the virtual work associated with the external load vector $\mathbf{f}$ comprising the axial distributed load p and transverse distributed load q as given by

$$\delta W_E = \int_0^L \delta \mathbf{d}^T \mathbf{f} \mathrm{d}x \tag{26}$$

with $\mathbf{f} = [p \quad q \quad 0]^{\mathrm{T}}$.

2.5 Material models

The comprehensive material laws are adopted to consider the material nonlinearity. Fig. 6(a) shows the model for concrete comprising the stress-strain envelope curve in compression developed by Attard and Setunge (1996) with parameters recommended by Attard and Stewart

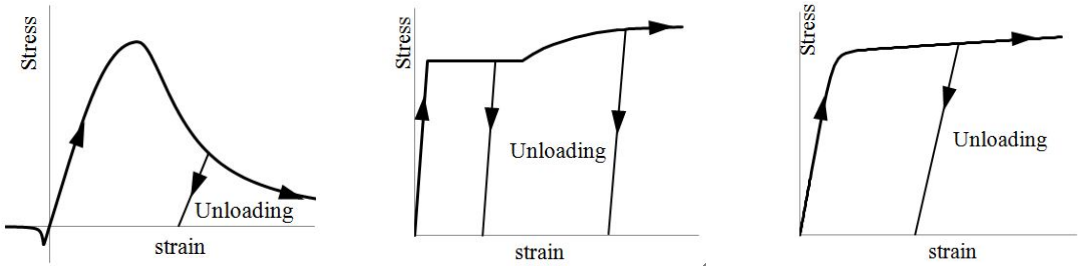

Fig. 6 Stress-strain curves of materials: (a) concrete; (b) non-prestressed steel; and (c) prestressing steel

(1998) and that in tension proposed by Carreira and Chu (1986), and Guo and Zhang (1987). The stress-strain curve recommended by Mander *et al*. (1984) is used for non-prestressed steel as shown in Fig. 6(b). The stress-strain formula for prestressing steel proposed by Menegotto and Pinto (1973) is adopted here as shown in Fig. 6(c). Although the original stress-strain formula of Menegotto and Pinto (1973) was proposed for reinforcing steel subjected to cyclic loading, Mattock (1979) and Naaman (1983) later proved that the formula also worked for prestressing steel.

3. Finite element formulation

To provide a tool for practical application to real bridges, a finite element model is formulated based on the theory proposed.

3.1 Beam finite element formulation

A C^1 three-node beam element (i.e., with shape functions having continuous first derivatives) is formulated as shown in Fig. 7. As the interior node has fewer degree of freedom compared with that of the edge node, the interior node is not suitable for use at diaphragms.

In the C^1 three-node beam element, the displacement vector **d** comprising the longitudinal displacement u of the beam axis, deflection v, and normal rotation φ are interpolated by linear, Hermite cubic, and quadratic polynomials respectively, namely

$$\mathbf{d}=\begin{Bmatrix} u \\ v \\ \varphi \end{Bmatrix}=\mathbf{N}\mathbf{d}^e=\begin{bmatrix} \mathbf{N}_u \\ \mathbf{N}_v \\ \mathbf{N}_\varphi \end{bmatrix}\mathbf{d}^e=\begin{bmatrix} N_{1u} & 0 & 0 & 0 & 0 & N_{u2} & 0 & 0 & 0 \\ 0 & N_{v1} & N_{v2} & 0 & 0 & 0 & N_{v3} & N_{v4} & 0 \\ 0 & 0 & 0 & N_{\varphi 1} & N_{\varphi 2} & 0 & 0 & 0 & N_{\varphi 3} \end{bmatrix}\mathbf{d}^e \tag{27}$$

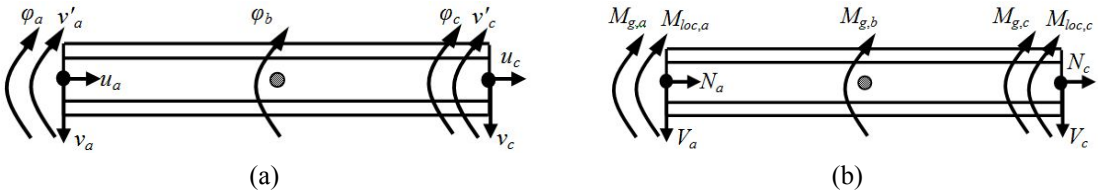

Fig. 7 A C^1 three-node beam element: (a) degrees of freedom; and (b) internal nodal forces

where the nodal displacement vector is $\mathbf{d}^e = \{u_a \;\; v_a \;\; v'_a \;\; \varphi_a \;\; \varphi_b \;\; u_c \;\; v_c \;\; v'_c \;\; \varphi_c\}^{\mathrm{T}}$ with the element nodes numbered locally as *a*, *b* and *c*; the shape function matrix **N** contains sub-matrices $\mathbf{N}_u$, N_v and $\mathbf{N}_\varphi$; $N_{u1} = 1 - \xi$; $N_{u2} = \xi$; $N_{v1} = 1 - 3\xi^2 + 2\xi$; $N_{v2} = (\xi - 2\xi^{2-} + \xi^3)L^e$; $N_{v3} = 3\xi^2 - 2\xi^3$; $N_{v4} = (-\xi^2 + \xi^3)L^e$; $N_{\varphi 1} = 1 - 3\xi + 2\xi^2$; $N_{\varphi 2} = 4\xi - 4\xi^2$; $N_{\varphi 3} = -\xi - 2\xi^2$; $\xi = (x - x_a) / L^e (0 \le \xi \le 1)$; the superscript *e* refers to the beam element; and L^e is the element length. In view of the shape functions adopted, the shear-related terms φ and $\partial v/\partial x$ as shown in Eq. (7) are both quadratic, and therefore shear locking can be avoided. That is why the proposed beam element has three nodes, with the interior node having fewer degrees of freedom.

It is assumed that the local and global strains increase simultaneously, and that the local and global stresses are distributed according to the corresponding strain ratios.

Combining Eqs. (3) and (7), the strain vector $\boldsymbol{\varepsilon}$ can be obtained as

$$\boldsymbol{\varepsilon} = \begin{bmatrix} \varepsilon_0 \\ \gamma \\ -\dfrac{\partial^2 v}{\partial x^2} \\ \dfrac{\partial \varphi}{\partial x} \end{bmatrix} = \begin{bmatrix} \dfrac{\partial u}{\partial x} + \dfrac{1}{2}\left(\dfrac{\partial v}{\partial x}\right)^2 \\ \varphi + \dfrac{\partial v}{\partial x} \\ -\dfrac{\partial^2 v}{\partial x^2} \\ \dfrac{\partial \varphi}{\partial x} \end{bmatrix} = \left\{ \mathbf{B}_l + \frac{1}{2}\mathbf{B}_{nl} \right\} \mathbf{d}^e \tag{28}$$

where the linear and nonlinear strain-displacement matrices $\mathbf{B}_l$ and $\mathbf{B}_{nl}$ are given respectively as

$$\mathbf{B}_l = \begin{bmatrix} \dfrac{\partial}{\partial x} & 0 & 0 \\ 0 & \dfrac{\partial}{\partial x} & 1 \\ 0 & -\dfrac{\partial^2}{\partial x^2} & 0 \\ 0 & 0 & \dfrac{\partial}{\partial x} \end{bmatrix} \begin{bmatrix} \mathbf{N}_u \\ \mathbf{N}_v \\ \mathbf{N}_\varphi \end{bmatrix}, \quad \text{and} \quad \mathbf{B}_{nl} = \begin{bmatrix} 1 \\ 0 \\ 0 \\ 0 \end{bmatrix} \left(\frac{\partial \mathbf{N}_v}{\partial x} \mathbf{d}^e \right)^{\mathrm{T}} \frac{\partial \mathbf{N}_v}{\partial x} \tag{29a}$$

The variation form of Eq. (28) is

$$\delta\boldsymbol{\varepsilon} = \left[\mathbf{B}_l + \mathbf{B}_{nl} \right] \delta \mathbf{d}^e \tag{30}$$

A typical cross section of bridge with arrangement of bonded prestressing and non-prestressed steel is shown in Fig. 8. The cross section is divided into a number of layers for analysis. The concrete strain in each layer is assumed to be uniformly distributed and equal to the strain at the centre of layer (Lou and Xiang 2006). According to section equilibrium conditions, the stress resultants *N*, M_g, M_{loc} and V_w can be expressed as follows.

$$N = \sum_i \sigma_{ci} A_{ci} + \sum_j \left(\sigma_{sj} - \sigma_{csj} \right) A_{sj} + \sum_k \left(\sigma_{bpk} - \sigma_{cbpk} \right) A_{bpk} \tag{31a}$$

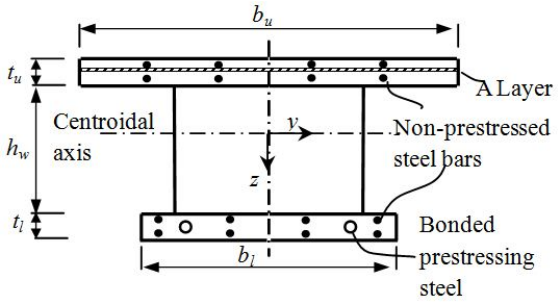

Fig. 8 Typical cross sections and simplified arrangement of steels of a bridge

$$M_g = \sum_i \sigma_{ci} A_{ci} e_f + \sum_j \left(\sigma_{sj} - \sigma_{csj}\right) A_{sj} e_f + \sum_k \left(\sigma_{bpk} - \sigma_{cbpk}\right) A_{bpk} e_f \tag{31b}$$

$$M_{loc} = \sum_i \sigma_{ci} A_{ci} \left(z_{ci} - e_f\right) + \sum_j \left(\sigma_{sj} - \sigma_{csj}\right) A_{sj} \left(z_{sj} - e_f\right) + \sum_k \left(\sigma_{bpk} - \sigma_{cbpk}\right) A_{bpk} \left(z_{bpk} - e_f\right) \tag{31c}$$

$$V_w = G_{eTw} A_w \gamma_w = G_{eTw} A_w \beta\gamma \tag{31d}$$

where σ, A and z correspond to stress, area and vertical coordinate respectively; subscripts *ci*, *sj* and *bpk* correspond to the *i*th concrete layer, *j*th ordinary reinforcing steel and *k*th bonded prestressing steel respectively; subscripts *csj* and *cbpk* correspond to concrete at the level of *j*th ordinary reinforcing steel and concrete at the level of *k*th bonded prestressing steel respectively; subscript *g* corresponds to the global bending of the flanges about the centroidal axis of the entire beam section assuming uniform strain in each flange; G_{eTw} is the tangent shear modulus of the corrugated steel webs considered as an equivalent orthotropic continuum; and subscript *loc* corresponds to the local bending of the flanges about their respective centroidal axes.

The differentials of Eqs. (31a) to (31d) are

$$\delta N = \sum_i E_{Tci} A_{ci} \delta\varepsilon_{ci} + \sum_j \left(E_{Tsj} - E_{Tcsj}\right) A_{sj} \delta\varepsilon_{sj} + \sum_k \left(E_{Tbpk} - E_{Tcbpk}\right) A_{bpk} \delta\varepsilon_{bpk} \tag{32a}$$

$$\delta M_g = \sum_i E_{Tci} A_{ci} e_f \delta\varepsilon_{ci} + \sum_j \left(E_{Tsj} - E_{Tcsj}\right) A_{sj} e_f \delta\varepsilon_{sj} + \sum_k \left(E_{Tbpk} - E_{Tcbpk}\right) A_{bpk} e_f \delta\varepsilon_{bpk} \tag{32b}$$

$$\begin{aligned} \delta M_{loc} = & \sum_i E_{Tci} A_{ci} \left(z_{ci} - e_f\right) \delta\varepsilon_{ci} + \sum_j \left(E_{Tsj} - E_{Tcsj}\right) A_{sj} \left(z_{sj} - e_f\right) \delta\varepsilon_{sj} \\ & + \sum_k \left(E_{Tbpk} - E_{Tcbpk}\right) A_{bpk} \left(z_{bpk} - e_f\right) \delta\varepsilon_{bpk} \end{aligned} \tag{32c}$$

$$\delta V_w = G_{eTw} A_w \delta\gamma_w = G_{eTw} A_w \beta\delta\gamma \tag{32d}$$

where E_T is the tangent modulus of material.

Substituting Eqs. (3) and (7) into Eq. (32a-d) yields the section tangent stiffness matrix $\mathbf{D}_T$ in terms of the internal force vector $\mathbf{F}_I$ as

$$\mathbf{D}_T = \delta\mathbf{F}_I / \delta\boldsymbol{\varepsilon} = \begin{bmatrix} d_{11} & d_{12} & d_{13} & d_{14} \\ & d_{22} & d_{23} & d_{24} \\ & Sym. & d_{33} & d_{34} \\ & & & d_{44} \end{bmatrix} \tag{33}$$

where

$$\mathbf{F}_I = \begin{bmatrix} N & V_w & M_{loc} & M_g \end{bmatrix}^{\mathrm{T}} \tag{34}$$

and the other elements are given by

$$d_{11} = \sum_i E_{Tci} A_{ci} + \sum_j \left(E_{Tsj} - E_{Tcsj} \right) A_{sj} + \sum_k \left(E_{Tbpk} - E_{Tcbpk} \right) A_{bpk} \; ; \quad d_{12} = 0 \; ;$$

$$d_{13} = \sum_i E_{Tci} A_{ci} \left(z_{ci} - e_f \right) + \sum_j \left(E_{Tsj} - E_{Tcsj} \right) A_{sj} \left(z_{sj} - e_f \right) + \sum_k \left(E_{Tbpk} - E_{Tcbpk} \right) A_{bpk} \left(z_{bpk} - e_f \right) ;$$

$$d_{14} = \sum_i E_{Tci} A_{ci} e_f + \sum_j \left(E_{Tsj} - E_{Tcsj} \right) A_{sj} e_f + \sum_k \left(E_{Tbpk} - E_{Tcbpk} \right) A_{bpk} e_f \; ;$$

$$d_{22} = G_{eTw} A_w \beta \; ; \quad d_{23} = 0 \; ; \quad d_{24} = 0 \; ;$$

$$d_{33} = \sum_i E_{Tci} A_{ci} \left(z_{ci} - e_f \right)^2 + \sum_j \left(E_{Tsj} - E_{Tcsj} \right) A_{sj} \left(z_{sj} - e_f \right)^2 + \sum_k \left(E_{Tbpk} - E_{Tcbpk} \right) A_{bpk} \left(z_{bpk} - e_f \right)^2$$

$$d_{34} = \sum_i E_{Tci} A_{ci} e_f \left(z_{ci} - e_f \right) + \sum_j \left(E_{Tsj} - E_{Tcsj} \right) A_{sj} e_f \left(z_{sj} - e_f \right) + \sum_k \left(E_{Tbpk} - E_{Tcbpk} \right) A_{bpk} e_f \left(z_{bpk} - e_f \right) ;$$

$$\text{and} \quad d_{44} = \sum_i E_{Tci} A_{ci} e_f^{\,2} + \sum_j \left(E_{Tsj} - E_{Tcsj} \right) A_{sj} e_f^{\,2} + \sum_k \left(E_{Tbpk} - E_{Tcbpk} \right) A_{bpk} e_f^{\,2} \; .$$

Introducing Eqs. (30) and (34) to the virtual strain energy of the beam in Eq. (8) yields

$$\delta U_b^e = \int_{L^e} \left(\delta\boldsymbol{\varepsilon} \right)^{\mathrm{T}} \mathbf{F}_I \mathrm{d}x = \int_{L^e} \left(\delta\mathbf{d}^e \right)^{\mathrm{T}} \left(\left[\mathbf{B}_l + \mathbf{B}_{nl} \right]^{\mathrm{T}} \right) \mathbf{F}_I \mathrm{d}x = \left(\delta\mathbf{d}^e \right)^{\mathrm{T}} \mathbf{f}_b^e \tag{35}$$

where the equivalent element nodal load vector $\mathbf{f}_b^e$ is given by

$$\mathbf{f}_b^e = \int_{L^e} \left(\left[\mathbf{B}_l + \mathbf{B}_{nl} \right]^{\mathrm{T}} \right) \mathbf{F}_I \mathrm{d}x \tag{36}$$

The differential $\mathrm{d}\mathbf{f}_b^e$ of Eq. (36) is

$$\mathrm{d}\mathbf{f}_b^e = \int_{L^e} \left(\mathbf{B}_l + \mathbf{B}_{nl} \right)^{\mathrm{T}} \mathrm{d}\mathbf{F}_I \mathrm{d}x + \int_{L^e} \left(\mathrm{d}\mathbf{B}_{nl} \right)^{\mathrm{T}} \mathbf{F}_I \mathrm{d}x \tag{37}$$

Substituting Eqs. (33)-(34) and (29b) into Eq. (37) yields the element tangent stiffness matrix as

$$\mathrm{d}\mathbf{f}_b^e = \mathbf{k}_b^e \mathrm{d}\mathbf{d}^e = \left(\mathbf{k}_l^e + \mathbf{k}_{nl}^e + \mathbf{k}_{gn}^e \right) \mathrm{d}\mathbf{d}^e \tag{38}$$

where $\mathbf{k}_b^e = \mathbf{k}_l^e + \mathbf{k}_{nl}^e + \mathbf{k}_{gn}^e$ is the tangent stiffness of the beam, which comprises $\mathbf{k}_l^e = \int_{L^e} (\mathbf{B}_l^T \mathbf{D}_T \mathbf{B}_l) \mathrm{d}x$; $\mathbf{k}_{nl}^e = \int_{L^e} (\mathbf{B}_{nl}^T \mathbf{D}_T \mathbf{B}_l + \mathbf{B}_l^T \mathbf{D}_T \mathbf{B}_{nl} + \mathbf{B}_{nl}^T \mathbf{D}_T \mathbf{B}_{nl}) \mathrm{d}x$; and $\mathbf{k}_{gn}^e = \int_{L^e} \left(\frac{\partial \mathbf{N}_v}{\partial x} \right)^{\mathrm{T}} \frac{\partial \mathbf{N}_v}{\partial x} N \mathrm{d}x$.

For the nonlinear case, the axial displacement u is coupled with the deflection v. To avoid possible membrane locking, it is desirable to have u' with the same order as $(v')^2$. In fact, unless a very high-order interpolation of u is used, e.g., Zona *et al*. (2008), the element will not satisfy the constraint. Another practical way to address the issue is to use the minimum interpolation of u and v, i.e., linear interpolation for u and Hermite cubic interpolation for v, but treating the strain of the beam axis ε_0 as a constant. Since u' is constant already, it is desirable to treat $(v')^2$ also as a constant in the numerical evaluation of the element stiffness. Thus, all nonlinear terms related to $(v')^2$ are evaluated using reduced integration by single-point Gaussian quadrature. All other terms are evaluated using exact integration, i.e., three-point Gaussian quadrature (Reddy 2004).

3.2 Modelling of diaphragm effects

From Eq. (17), the virtual strain energy $\delta U_{dia,k}$ of the k-th diaphragm located at an edge node can be given by

$$\begin{aligned} \delta U_{dia,k} &= \left\{ \left[K_d h_w \beta \left(\varphi + \frac{\partial v}{\partial x} \right) h \right] \left(\delta\varphi + \frac{\partial \delta v}{\partial x} \right) \right\}_{x=x_k} \\ &= \left(\mathbf{d}_k\right)^{\mathrm{T}} \begin{bmatrix} 0 & 0 & 1 & 1 \end{bmatrix}^{\mathrm{T}} K_d h^2 \begin{bmatrix} 0 & 0 & 1 & 1 \end{bmatrix} \delta \mathbf{d}_k = \mathbf{f}_{d,k} \delta \mathbf{d}_k \end{aligned} \tag{39}$$

where x_k is the x-value of the k-th diaphragm; $\mathbf{d}_k$ is the displacement vector of the edge node; and $\mathbf{f}_{d,k}$ is the force couple vector that the diaphragm transmits to the beam and given by $\mathbf{f}_{d,k} = (\mathbf{d}_k)^{\mathrm{T}}[0\ 0\ 1\ 1]^{\mathrm{T}}\ K_d h^2\ [0\ 0\ 1\ 1]$. The tangent stiffness matrix $\mathbf{k}_{dia,k}$ contributed by the k-th diaphragm is given by

$$\mathbf{k}_{dia,k} = \partial \mathbf{f}_{d,k} / \partial \mathbf{d}_k \tag{40}$$

If the diaphragm is thick, it can be modelled by several beam elements with solid section along the span. For practicality, the solid section can be divided into hypothetical flanges and thick concrete web for modelling of their bending and shear rigidities.

3.3 Finite element formulation of external tendons

The deformation of external tendon given by Eq. (23) depends on the displacements of anchorages and deviators. It is assumed that the positions of the (n+1) deviators or anchorages coincide with some of the en edge nodal points of the mesh. Consequently, the virtual strain $\delta\varepsilon_p$ of the external tendon is given by

$$\delta\varepsilon_p = \frac{1}{L_{t0}} \sum_{j=1}^{n} \left\{ \frac{\left(\Delta_j e + \Delta_j v\right)}{l_{p,j}} \Delta_j \delta v + \frac{\Delta_j x}{l_{p,j}} \left[\Delta_j \delta u + \Delta_j \left(e \delta\varphi \right) \right] \right\} = \frac{1}{L_{t0}} \boldsymbol{\chi} \delta \mathbf{D} \tag{41a}$$

where $\mathbf{D}$ is the global nodal displacement vector of the beam; and the kinematic compatibility vector of the external tendon for expanding to cope with the global displacement vector is $\boldsymbol{\chi} = [\chi_1$

$0\ \ \boldsymbol{\chi}_2\ \ 0\ \ \cdots\ \ \boldsymbol{\chi}_{en-1}\ \ 0\ \ \boldsymbol{\chi}_{en}]$ with

$$\boldsymbol{\chi}_i=\begin{cases}0_{1\times 4} \ \text{ when } \ x_i\neq x_j\ (j=0,1,2,...,n)\\ \left[-\dfrac{\Delta_1 x}{l_{p,1}}\ -\dfrac{\Delta_1 e+\Delta_1 v}{l_{p,1}}\ 0\ -e_0\dfrac{\Delta_1 x}{l_{p,1}}\right] \text{ when } \ x_i=x_j(j=0)\\ \left[\dfrac{\Delta_j x}{l_{p,j}}-\dfrac{\Delta_{j+1}x}{l_{p,j+1}}\ \dfrac{\Delta_j e+\Delta_j v}{l_{p,j}}-\dfrac{\Delta_{j+1}e+\Delta_{j+1}v}{l_{p,j+1}}\ 0\ e_j\left(\dfrac{\Delta_j x}{l_{p,j}}-\dfrac{\Delta_{j+1}x}{l_{p,j+1}}\right)\right]\\ \qquad \text{when } \ x_i=x_j(j=1,2,...,n-1)\\ \left[\dfrac{\Delta_n x}{l_{p,n}}\ \dfrac{\Delta_n e+\Delta_n v}{l_{p,n}}\ 0\ e_n\dfrac{\Delta_n x}{l_{p,n}}\right] \text{ when } \ x_i=x_j(j=n)\end{cases} \tag{41b}$$

In the kinematic compatibility vector $\boldsymbol{\chi}$, the sub-vector $\boldsymbol{\chi}_i$ corresponds to the i-th edge nodal point with abscissa x_i while each zero between sub-vectors corresponds to an interior node of three-node beam element. As the external tendon is in contact with the beam only at the anchorages and deviators, components of the kinematic compatibility vector $\boldsymbol{\chi}$ are zero except for those corresponding to the edge nodal points with anchorages or deviators. Hence, the virtual work δU_p done by the external tendon can be written as

$$\delta U_p=L_{t0}A_p\sigma_p\delta\varepsilon_p=A_p\sigma_p\boldsymbol{\chi}\delta\mathbf{D}=\mathbf{F}_p\delta\mathbf{D} \tag{42}$$

where A_p is the cross sectional area of tendon, σ_p is the tendon stress, and the equivalent load vector $\mathbf{F}_p$ comprises the forces that the external tendon transmits to the beam as given by $A_p\sigma_p\boldsymbol{\chi}$. The tangent stiffness matrix $\mathbf{K}_p$ contributed by the external tendon is

$$\mathbf{K}_p=\frac{\partial\mathbf{F}_p}{\partial\mathbf{D}}=\frac{\partial\left(A_p\sigma_p\boldsymbol{\chi}\right)}{\partial\mathbf{D}}=A_p\frac{\partial\sigma_p}{\partial\varepsilon_p}\frac{1}{L_{t0}}\boldsymbol{\chi}^{\mathrm{T}}\boldsymbol{\chi}+A_p\sigma_p\frac{\partial\boldsymbol{\chi}}{\partial\mathbf{D}} \tag{43}$$

For simplification, only one resultant external tendon is considered hereafter. Straightforward generalization to the case of multiple external tendons may be obtained by assembling the tangent stiffness matrices of other external tendons.

3.4 Global finite element modelling

In accordance with the conventional finite element formulation, the global stiffness equation is obtained as

$$\mathbf{K}\delta\mathbf{D}=\delta\mathbf{F} \tag{44}$$

where the global stiffness $\mathbf{K}$ comprises the global beam stiffness matrix $\mathbf{K}_b$, the global stiffness matrix due to external tendon $\mathbf{K}_p$ and the global stiffness matrix due to diaphragms $\mathbf{K}_{dia}$, i.e., $\mathbf{K}=\mathbf{K}_b+\mathbf{K}_p+\mathbf{K}_{dia}$; $\mathbf{K}_b=\sum_e\mathbf{k}_b^e$; $\mathbf{K}_{dia}=\sum_k\mathbf{k}_{dia,k}$; $\mathbf{F}$ is the global nodal force vector of the beam; and $\sum(\,)$ denotes the assembly process. In the tendon-beam finite element model, the effects of diaphragm and external tendon can be obtained directly.

3.5 Solution algorithm

Since the system is nonlinear, an iterative method must be used for the solution. The constant arc-length technique is adopted in this paper. The constant arc-length is an elliptic condition limiting the loading and displacement of an increment. Appropriate load increments are selected automatically depending on the current stiffness of the structure. The algorithm is not only more stable, but it also improves the convergence efficiency due to higher flexibility in adjusting the applied load. Within each increment, the iteration is carried out by the modified Newton-Raphson method.

4. Verification by experimental tests

4.1 Experimental programme

Some prestressed concrete beam specimens with corrugated steel web with different arrangements of prestressing and loading were fabricated for testing to verify the numerical model proposed. The test arrangements of Specimens "A-1", "B-1", "B-2" and "P-1" are shown in Figs. 9 to 12 respectively and summarised in Table 1. Specimens A-1, B-1 and B-2 were post-tensioned by two external 7-wire steel strands. Specimen P-1 was pre-tensioned by two bonded 7-wire steel strands. Specimens A-1 and P-1 were 4700 mm in length, 300 mm in depth with single 5 mm thick corrugated steel web and simply supported over a span of 4500 mm. Specimens B-1 and B-2 were both 3800 mm in length, 360 mm in depth with single 5 mm thick corrugated steel web and simply supported over a span of 3600 mm. The flanges of these four specimens were cast of high strength concrete with design cube strength of 65 MPa. Embedment connections were provided between the concrete flanges and corrugated steel web. The anchorages of Specimens A-1 and B-2 were located at the centroid of the 200 mm thick end diaphragms and the strands at intermediate deviator were 70 mm and 100 mm, respectively, above the soffit. In Specimen B-1, the anchorages of straight strands were located at a level 110 mm above the soffit at the end diaphragms. The straight prestressing strands of Specimen P-1 were located inside the lower flange at a level 20 mm above the soffit. To prevent any bond-slip between the prestressing tendons and their surrounding concrete, there were additional anchorages at the ends of Specimen P-1. The thicknesses of intermediate diaphragms of these specimens were 90 mm.

Chen *et al*. (2015a) have undertaken an extensive parametric study to clarify the effects of various parameters such as the section shape, grade of concrete, steel content, prestressing force ratio of bonded tendons, etc. on the sectional ductility, deformability and strength of this type of bridges. However, the use of external prestressing implies that the structural behaviour is governed not only by individual sections, but also by the overall global structural behaviour because of the unbonded nature of external tendons. In particular, Specimens A-1 and P-1 had the same configuration and material properties, but different prestressing arrangements, and they were both tested by third-point loading. In comparison, Specimens B-1 and B-2 were less slender. These two specimens had the same section and material properties, but different profiles of external prestressing strands. They were tested by point loading at mid-span.

The effective prestressing forces of Specimens A-1, B-1, B-2 and P-1 were 191 kN, 268 kN, 252 kN and 186 kN respectively. The specimens were tested under displacement control. Load cells were used at the end of each tendon to monitor the variation of tendon force during tensioning and the subsequent loading test. Linear variable differential transformers (LVDTs) were

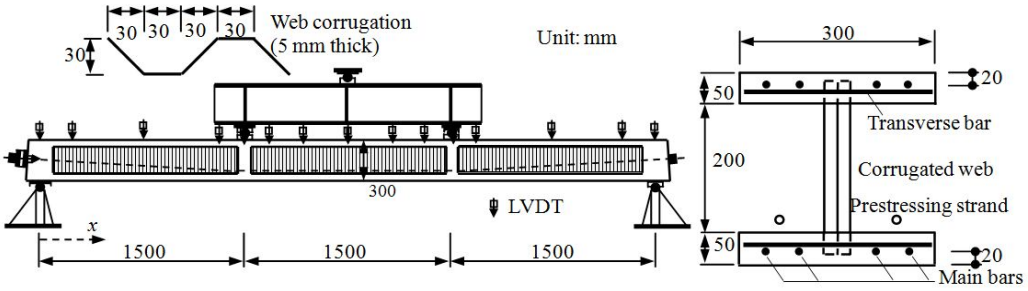

Fig. 9 Test of Specimen A-1

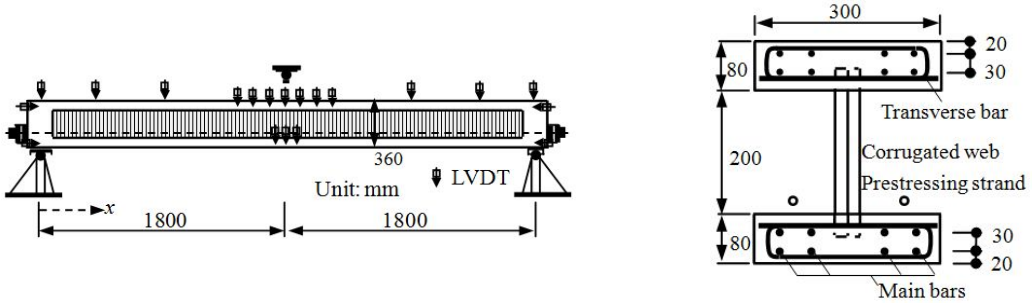

Fig. 10 Test of Specimen B-1

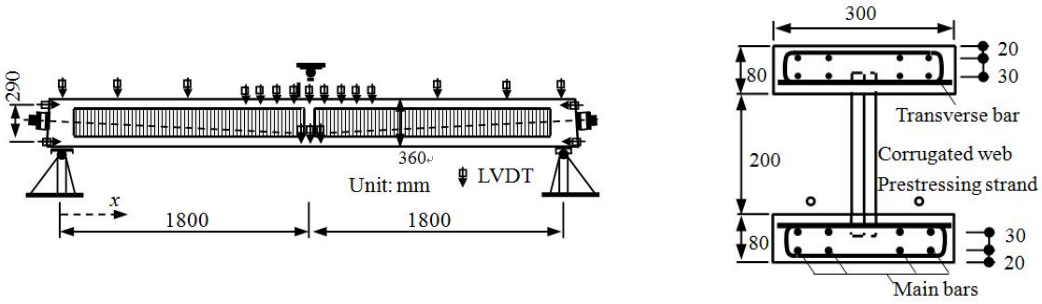

Fig. 11 Test of Specimen B-2

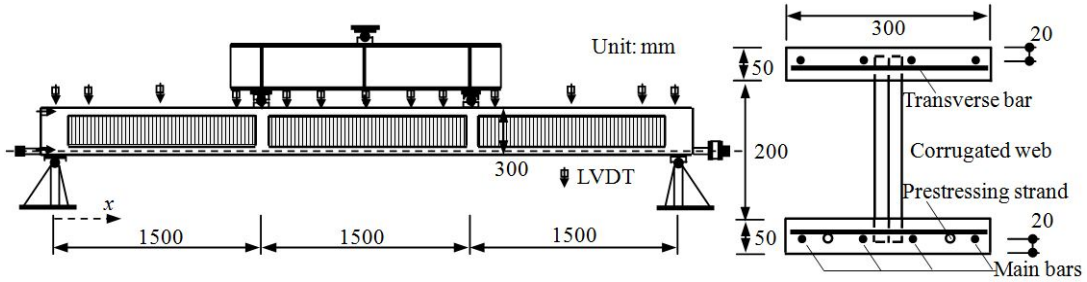

Fig. 12 Test of Specimen P-1

Table 1 Design of specimens tested

Specimen No.	Span (mm)	Beam depth (mm)	Flange thickness (mm)	Web thickness (mm)	End diaphragm thickness (mm)	Intermediate diaphragm thickness (mm)	Tendon type	No. of deviators	Loading point(s)
A-1	4500	300	50	5	200	70	External	2	Third points
B-1	3600	360	80	5	200	-	External	0	Mid-span
B-2	3600	360	80	5	200	70	External	1	Mid-span
P-1	4500	300	50	5	200	70	Internal (bonded)	2	Third points

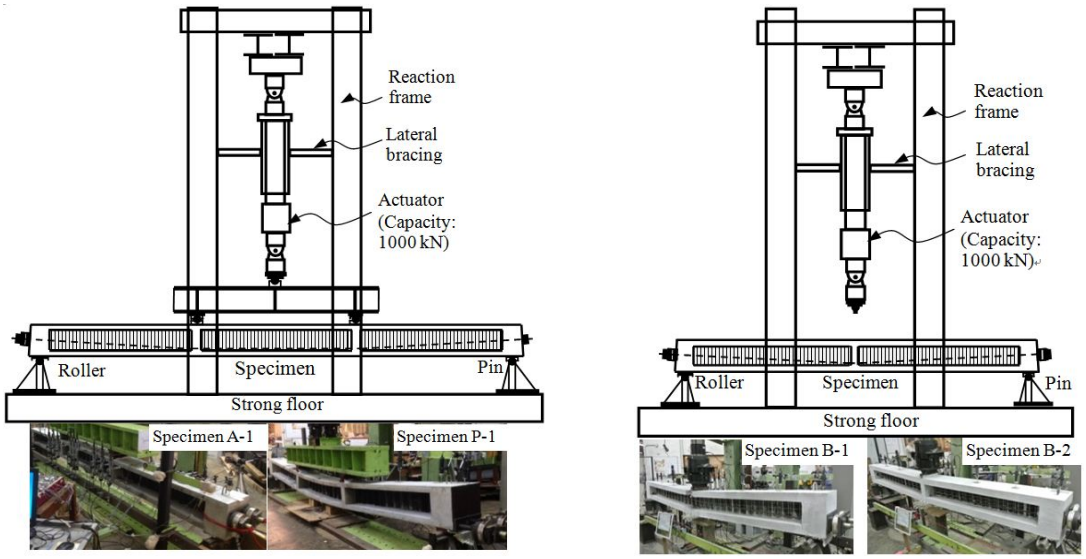

(a) (b)

Fig. 13 Test setup of specimens tested: (a) Specimens A-1 and P-1; and (b) Specimens B-1 and B-2

used to measure displacements during the test. The test setup of these four specimens is shown in Fig. 13.

Routine tests of the materials were carried out to determine the properties of materials, which are shown in Table 2.

4.2 Experimental results

The load-deflection curves of Specimens A-1, B-1, B-2 and P-1 obtained experimentally and numerically as shown in Fig. 14 show reasonably good agreement as confirmed by the percentage errors given in Table 3. The load-deflection curves clearly exhibit three stages, namely (a) elastic, (b) cracked-elastic, and (c) plastic. The transition from the first stage to the second stage is due to the cracking of concrete, while the transition to the third stage is caused by yielding of the non-prestressed steel in the lower flange. Finally, due to the crushing of concrete and buckling of compression steel bars of the upper flange, the specimens failed as shown in Fig. 14. In the plastic

Table 2 Material properties from tests (unit: MPa)

Specimen No.	Concrete		Steel reinforcement (10 mm diameter bar)		
	Initial Young's modulus	Cube strength	Initial Young's modulus	Yield strength	Ultimate strength
A-1	29709	65.0	192277	559	672
B-1	26107	54.3			
B-2	27606	61.3			
P-1	30962	67.7			
Specimen No.	Prestressing tendon (12.7 mm strand)		Steel web		
	Initial Young's modulus	Ultimate strength	Initial Young's modulus	Yield strength	Ultimate strength
A-1	206780	2008	196056	267	399
B-1					
B-2					
P-1					

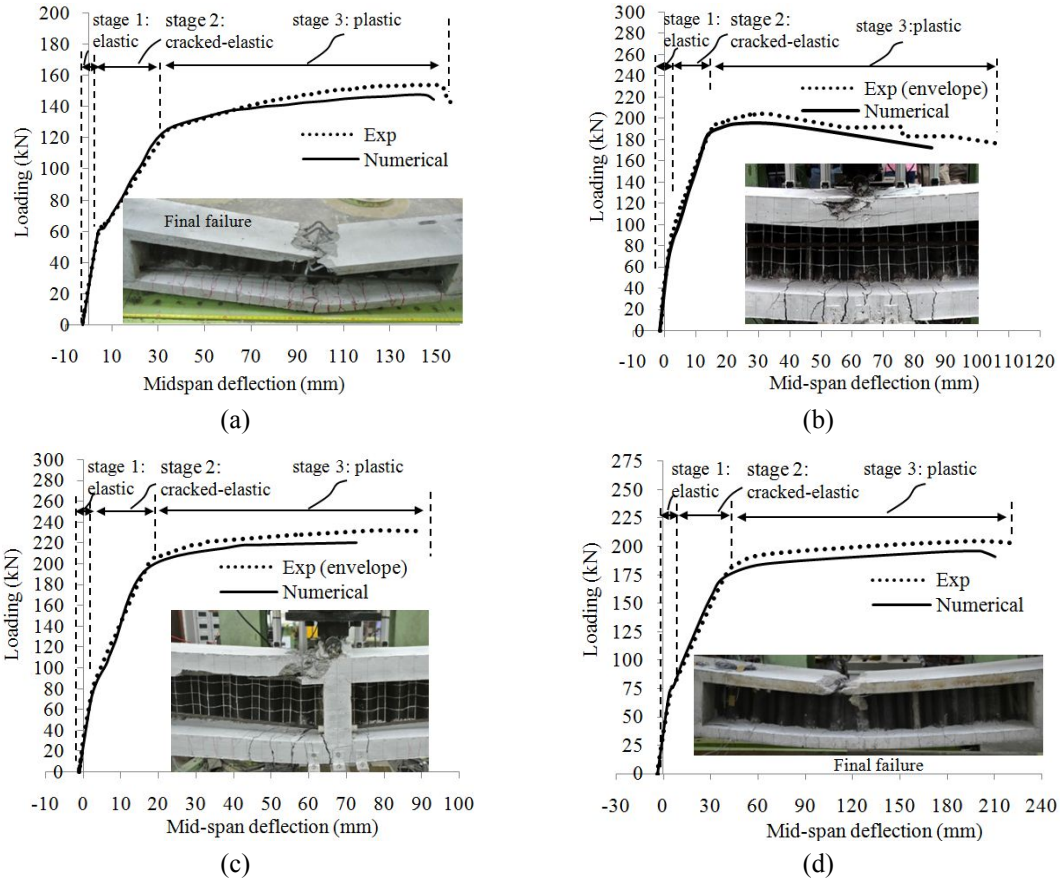

Fig. 14 Load-deflection curves of specimens tested: (a) Specimen A-1; (b) Specimen B-1; (c) Specimen B-2; and (d) Specimen P-1

stage, the corrugated steel web was stretched significantly and could take part of the bending moment, possibly causing the discrepancy in numerical prediction of ultimate load. The measured and predicted values of tendon stress of Specimens A-1, B-1 and B-2 in Fig. 15 show reasonably good agreement as confirmed in Table 3. With the increase of applied loading and the specimen progresses from the elastic stage to plastic stage, the effects of diaphragm and interaction become less significant due to the plastic behaviour of materials. Specimens B-1 and B-2 were tested by cyclic loading to and unloading from increasing ductility levels, and hence the experimental results of Specimens B-1 and B-2 in Figs. 14 and 15 are the hysteresis envelopes.

Table 3 Errors of numerical results based on the same displacement

Specimen No.	Worst error of applied force			Worst error of tendon stress		
	At elastic stage	At cracked elastic stage	At plastic stage	At elastic stage	At cracked elastic stage	At plastic stage
A-1	1.7%	4.6%	-6.2%	0.5%	0.8%	0.3%
B-1	-6.4%	-6.9%	-6.2%	0.0%	0.1%	1.1%
B-2	-4.5%	-6.7%	-5.3%	0.4%	0.4%	0.0%
P-1	4.0%	4.4%	-4.2%	-	-	-

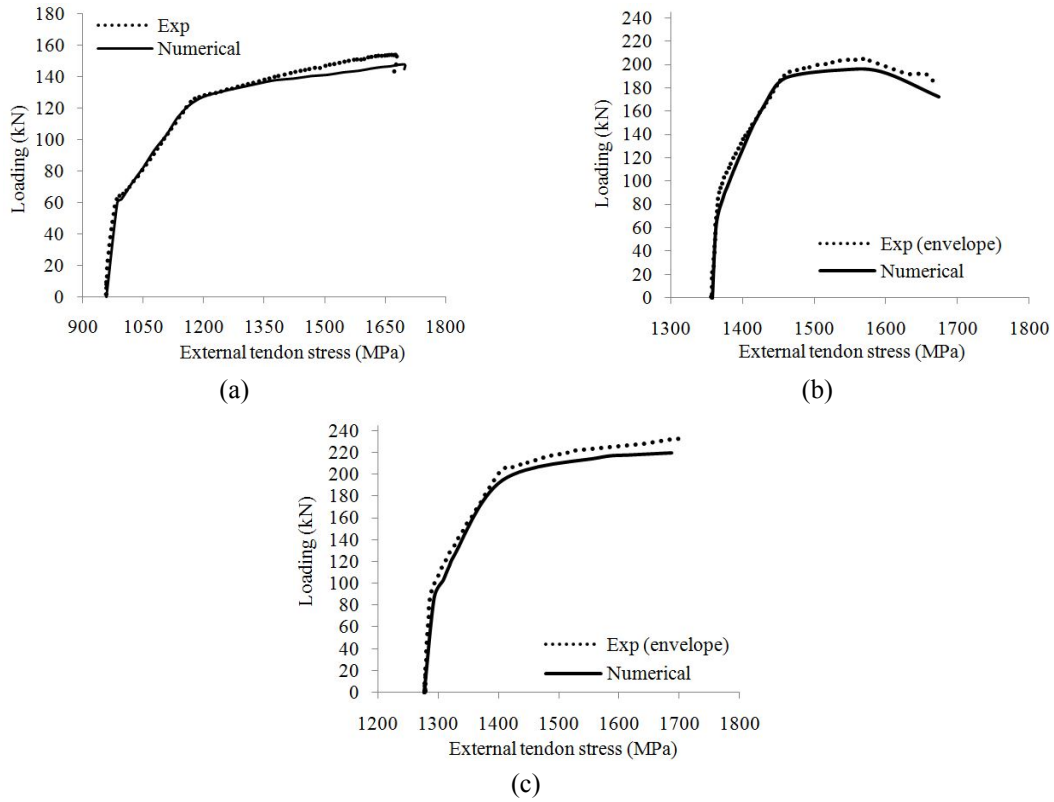

Fig. 15 Variation of tendon stress of specimens tested: (a) Specimen A-1; (b) Specimen B-1; and (c) Specimen B-2

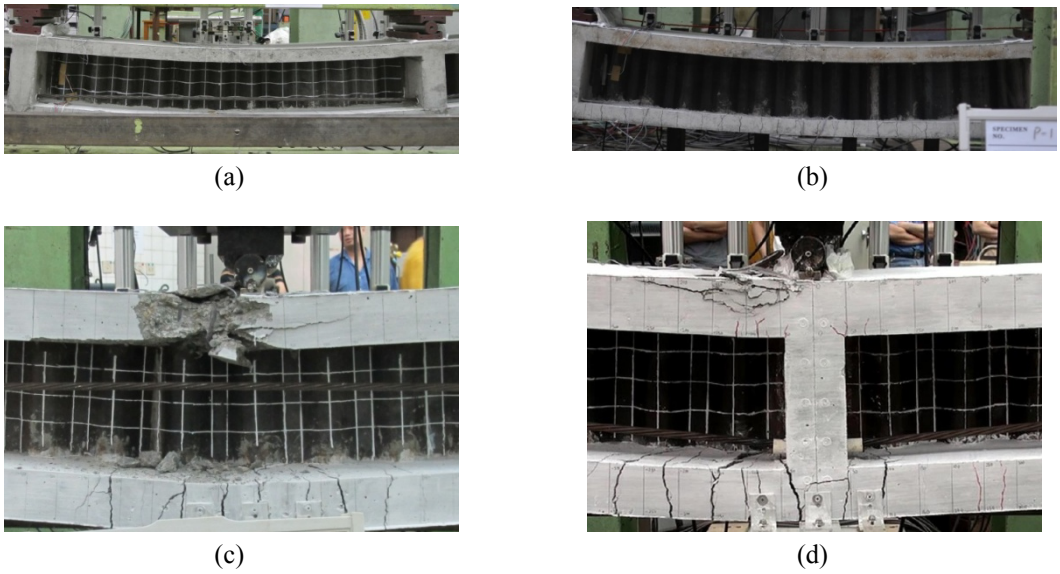

(a) (b)

(c) (d)

Fig. 16 Deformation around mid-span of specimens tested: (a) Specimen A-1; (b) Specimen P-1; (c) Specimen B-1; and (d) Specimen B-2

The nonlinear numerical analysis was carried out in three phases: (a) beam under self-weight; (b) prestressing of beam under self-weight; and (c) application of loading on the beam until failure. The initial Young's modulus of concrete was taken as the measured value instead of that proposed by Attard and Setunge (1996) because of the use of relative soft local aggregate in Hong Kong.

The displacement ductility factors of Specimens A-1, B-1, B-2 and P-1 were evaluated as 3.37, 7.0, 4.5 and 4.79 respectively according to the practice of Park (1988) and Du *et al*. (2008). The ultimate loads of Specimens A-1, B-1, B-2 and P-1 were measured as 154 kN, 205 kN, 233 kN and 205 kN respectively. The lower ultimate load of Specimen A-1 compared with Specimen P-1 is caused by the external prestressing system that allows relative slipping between the tendons and deviators as well as the second-order effect because of the reduction of eccentricity of external tendons due to beam deflection. The lower ultimate load of Specimen B-1 as compared with that of Specimen B-2 is similarly due to the second-order effect associated with external tendons. In the plastic stage, the reduction of eccentricity due to second-order effects of external tendon become very significant as shown in Figs. 16(a) and (c), which reduce the ultimate load.

5. Conclusions

The present study extends the sandwich beam theory to predict the full-range behaviour of prestressed concrete bridges with corrugated steel webs taking into account the interaction between the girder, diaphragms and external tendons. The model considers the geometric nonlinearity and the actual stress-strain curves as well as strain reversals. The interaction between external tendons and the girder is modelled by nonlinear kinematical theory. A nonlinear finite element method is developed accordingly. The numerical model is verified by experiments. The load-deflection curves of tested specimens clearly exhibit three stages, i.e., elastic, cracked-elastic and plastic stages. As deformation of the beam increases, the stresses of external tendons increase,

which in turn help to resist loading. The proposed model can predict both the linear and nonlinear behaviour of this form of bridges.

Acknowledgments

The work reported in this paper is supported by the Research Grants Council (RGC) of the Hong Kong Special Administrative Region, China (RGC Project No. HKU 710111E).

References

Attard, M.M. and Setunge, S. (1996), "The stress-strain relationship of confined and unconfined concrete", *ACI Mater. J.*, **93**(5), 432-442.

Attard, M.M. and Stewart, M.G. (1998), "A two parameter stress block for high-strength concrete", *ACI Struct. J.*, **95**(3), 305-317.

Au, F.T.K., Du, J.S. and Cheung, Y.K. (2005), "Service load behavior of unbonded partially prestressed concrete members", *Mag. Concr. Res.*, **57**(4), 199-209.

Barakat, S., Al Mansouri, A. and Altoubat, S. (2015), "Shear strength of steel beams with trapezoidal corrugated webs using regression analysis", *Steel Compos. Struct., Int. J.*, **18**(3), 757-773.

Bariant, J.F. and Utsunomiya, T. (2006), "Watanabe E. Elasto-plastic analysis of PC girder with corrugated steel web by an efficient beam theory", *Struct. Eng. / Earthq. Eng. JSCE*, **23**(2), 257s-268s.

Briassoulis, D. (1986), "Equivalent orthotropic properties of corrugated sheets", *Comput. Struct.*, **23**(2), 129-138.

Carreira, D.J. and Chu, K.H. (1986), "The moment-curvature relationship of reinforced concrete members", *ACI Struct. J.*, **83**(2), 191-198.

Chen, X.C., Au, F.T.K., Bai, Z.Z., Li, Z.H. and Jiang, R.J. (2015a), "Flexural ductility of reinforced and prestressed concrete sections with corrugated steel webs", *Comput. Concrete*, **16**(4), 625-642.

Chen, X.C., Bai, Z.Z., Au, F.T.K. and Zeng, Y. (2015b), "An extended sandwich theory for prestressed concrete bridges with corrugated steel web(s)", *Report of IABSE Conference on* "*Elegance in Structures*", Nara, Japan, May.

Cheyrezy, M. and Combault, J. (1990), "Composite bridges with corrugated steel webs - achievements and prospects", *Proceedings of IABSE Symposium on Mixed Structures including New Materials*, Brussels, Belgium, September.

Dall'Asta, A., Ragni, L. and Zona, A. (2007), "Analytical model for geometric and material nonlinear analysis of externally prestressed beams", *J. Eng. Mech.*, **133**(1), 117-121.

Du, J.S., Au, F.T.K., Cheung, Y.K. and Kwan, A.K.H. (2008), "Ductility analysis of prestressed concrete beams with unbonded tendons", *Eng. Struct.*, **30**(1), 13-21.

Eslami, A. and Ronagh, H.R. (2014), "Effect of elaborate plastic hinge definition on the pushover analysis of reinforced concrete buildings", *Struct. Des. Tall Spec. Build.*, **23**(4), 254-271.

Guo, Z.H. and Zhang, X.Q. (1987), "Investigation of complete stress-deformation curves for concrete in tension", *ACI Mater. J.*, **84**(4), 278-285.

Ho, J.C.M. and Pam, H.J. (2003), "Inelastic design of low-axially loaded high-strength reinforced concrete columns", *Eng. Struct.*, **25**(8), 1083-1096.

Johnson, R.P. and Cafolla, J. (1997), "Corrugated webs in plate girders for bridges", *Proc. ICE Struct. Build.*, **122**(2), 157-164.

Kato, H., Kawabata, A. and Nishimura, N. (2002), "Practical calculation formula on displacements and stress resultants of steel-concrete mixed girders with corrugated steel web", *Proceedings of JSCE*, **703**, 293-300. [In Japanese]

Ko, H.J., Moon, J., Shin, Y.W. and Lee, H.E. (2013), "Non-linear analyses model for composite box-girders with corrugated steel webs under torsion", *Steel Compos. Struct., Int. J.*, **14**(5), 409-429.

Kosa, K., Awane, S., Uchino, H. and Fujibayashi, K. (2006), "Ultimate behavior of prestressed concrete bridge with corrugated steel webs using embedded connection", *Proceedings of JSCE*, *Division E*, **62**(1), 202-220. [In Japanese]

Lou, T.J. and Xiang, Y.Q. (2006), "Finite element modelling of concrete beams prestressed with external tendons", *Eng*. *Struct*., **28**(14), 1919-1926.

Machimdamong, C., Watanabe, E. and Ustunomiya, T. (2004), "Analysis of corrugated steel web girders by an efficient beam bending theory", *Struct*. *Eng*. / *Earthq*. *Eng*. *JSCE*, **21**(2), 131s-142s.

Mander, J.B., Priestley, M.J.N. and Park, R. (1984), "Seismic design of bridge piers", Research Report 84-2; Department of Civil Engineering, University of Canterbury, Christchurch, New Zealand.

Mattock, A.H. (1979), "Flexural strength of prestressed concrete sections by programmable calculator", *J*. *Prestressed Concrete Institute*, **24**(1), 32-54.

Menegotto, M. and Pinto, P.E. (1973), "Method of analysis for cyclically loaded R.C. plane frames", *IABSE Preliminary Report for Symposium on Resistance and Ultimate Deformability of Structures Acted on by Well Defined Repeated Loads*, Lisbon, Portugal.

Mizuguchi, K., Ashiduka, K., Yoda, T., Sato, K., Sakurada, M. and Hidaka, S. (1998), "Loading tests of Hondani Bridge", *Bridge Found*. *Eng*., **32**(10), 25-34. [In Japanese]

Mo, Y.L., Jeng, C.H. and Krawinkler, H. (2003), "Experimental and analytical studies of innovative prestressed concrete box-girder bridges", *Mater*. *Struct*., **36**(2), 99-107.

Naaman, A.E. (1983), "An approximate nonlinear design procedure for partially prestressed concrete beams", *Comput*. *Struct*., **17**(2), 287-299.

Park, R. (1988), "Ductility evaluation from laboratory and analytical testing", *Proceedings of the 9th World Conference on Earthquake Engineering*, *VIII*, Kyoto, Japan, August.

Park, R. and Paulay, T. (1975), *Reinforced Concrete Structures*, John Wiley & Sons, Inc., New York, NY, USA.

Reddy, J.N. (2004), *An Introduction to Nonlinear Finite Element Analysis*, Oxford, New York, USA.

Research Group of Composite Structure with Corrugated Steel Web (1998), Design Manual of PC Box Girders with Corrugated Steel Webs; Tokyo, Japan. [In Japanese]

Samanta, A. and Mukhopadhyay, M. (1999), "Finite element static and dynamic analysis of folded plates", *Eng*. *Struct*., **21**(3), 277-287.

Taniguchi, N. and Yoda, T. (1997), "Study on a simple method for bending analysis of composite girders with corrugated steel webs", *Struct*. *Eng*. / *Earthq*. *Eng*. *JSCE*, **577**, 107-120.

Timoshenko, S.P. and Gere, J.M. (1972), *Mechanics of Materials*, Van Nostrand Reinhold, New York, NY, USA.

Xu, D., Ni, Y.S. and Zhao, Y. (2015), "Analysis of corrugated steel web beam bridges using spatial grid modelling", *Steel Compos*. *Struct*., *Int*. *J*., **18**(4), 853-871.

Youssf, O., ElGawady, M.A. and Mills, J.E. (2015), "Displacement and plastic hinge length of FRP-confined circular reinforced concrete columns", *Eng*. *Struct*., **101**, 465-476.

Zona, A. and Ranzi, G. (2011), "Finite element models for nonlinear analysis of steel concrete composite beams with partial interaction in combined bending and shear", *Finite Elem*. *Anal*. *Des*., **47**(2), 98-118.

Zona, A., Ragni, L. and Dall' Asta, A. (2008), "Finite element formulation for geometric and material nonlinear analysis of beams prestressed with external slipping tendons", *Finite Elem*. *Anal*. *Des*., **44**(15), 910-919.

CC